© 2014. Published by The Company of Biologists Ltd | Journal of Cell Science (2014) 127, 2782–2792 doi:10.1242/jcs.150011

RESEARCH ARTICLE

Bcl-2 binds to and inhibits ryanodine receptors

Tim Vervliet[1], Elke Decrock[2], Jordi Molgó[3], Vincenzo Sorrentino[4], Ludwig Missiaen[1], Luc Leybaert[2], Humbert De Smedt[1], Nael Nadif Kasri[5], Jan B. Parys[1] and Geert Bultynck[1,*]

ABSTRACT

The anti-apoptotic B-cell lymphoma-2 (Bcl-2) protein not only counteracts apoptosis at the mitochondria by scaffolding pro-apoptotic Bcl-2-family members, but also acts at the endoplasmic reticulum, thereby controlling intracellular Ca^{2+} dynamics. Bcl-2 inhibits Ca^{2+} release by targeting the inositol 1,4,5-trisphosphate receptor (IP_3R). Sequence analysis has revealed that the Bcl-2-binding site on the IP_3R displays strong similarity with a conserved sequence present in all three ryanodine receptor (RyR) isoforms. We now report that Bcl-2 co-immunoprecipitated with RyRs in ectopic expression systems and in native rat hippocampi, indicating that endogenous RyR–Bcl-2 complexes exist. Purified RyR domains containing the putative Bcl-2-binding site bound full-length Bcl-2 in pulldown experiments and interacted with the BH4 domain of Bcl-2 in surface plasmon resonance (SPR) experiments, suggesting a direct interaction. Exogenous expression of full-length Bcl-2 or electroporation loading of the BH4 domain of Bcl-2 dampened RyR-mediated Ca^{2+} release in HEK293 cell models. Finally, introducing the BH4-domain peptide into hippocampal neurons through a patch pipette decreased RyR-mediated Ca^{2+} release. In conclusion, this study identifies Bcl-2 as a new inhibitor of RyR-based intracellular Ca^{2+}-release channels.

KEY WORDS: Ca^{2+} signaling, Bcl-2, Ryanodine receptor, Hippocampus

INTRODUCTION

The B-cell lymphoma-2 (Bcl-2) family of proteins consists of both anti- and pro-apoptotic family members. To exert their function, Bcl-2-family members depend on the presence of one or more Bcl-2-homology (BH) domains (Letai, 2008). The role of anti-apoptotic Bcl-2 proteins, which contain four BH domains, as crucial gate keepers of mitochondrial outer-membrane integrity has been well established (Brunelle and Letai, 2009; Chipuk and Green, 2008). This is achieved by scaffolding and neutralizing pro-apoptotic proteins, like Bax and/or Bak and BH3-only proteins, through the hydrophobic cleft, which is formed by the BH3, BH1 and BH2 domains. It has become increasingly clear that Bcl-2 proteins also modulate intracellular Ca^{2+} signaling events by directly targeting Ca^{2+} transport mechanisms at different cellular locations. At the level of the endoplasmic reticulum (ER), the main intracellular Ca^{2+} store, Bcl-2-family members target the inositol 1,4,5-trisphosphate (IP_3) receptor (IP_3R) (Monaco et al., 2012a; Oakes et al., 2005; Rong et al., 2008; White et al., 2005), sarco/endoplasmic-reticulum Ca^{2+}-ATPases (SERCAs) (Kuo et al., 1998) and Bax inhibitor 1 (BI-1, also known as TMBIM6) (Ahn et al., 2010; Xu and Reed, 1998). At the mitochondrial outer membranes, Bcl-2 proteins target the voltage-dependent anion channels (VDACs) (Arbel and Shoshan-Barmatz, 2010; Arbel et al., 2012; Plötz et al., 2012). More recently, Bcl-2 has been shown to regulate plasma-membrane Ca^{2+}-ATPase (PMCA) activity (Ferdek et al., 2012). Therefore, the function of Bcl-2 in cells seems to be tightly linked to its ability to modulate intracellular Ca^{2+} homeostasis and dynamics. This is important, given the central role of both Bcl-2 and of Ca^{2+} signaling in cell-fate decisions, mitochondrial bioenergetics, autophagy, ER stress and apoptosis (Chipuk et al., 2010; Giorgi et al., 2008; Kiviluoto et al., 2013). Recent evidence indicates that the regulation of intracellular Ca^{2+} handling by Bcl-2-family proteins is also important for non-apoptotic functions, including neuroplasticity, cellular migration, cell cycle regulation and embryonic development (Bonneau et al., 2013).

The molecular determinants underlying the formation of the IP_3R–Bcl-2 complex have been identified (Rong et al., 2009; Rong et al., 2008). The BH4 domain of Bcl-2 has been shown to be responsible for binding to a stretch of 20 amino acids located in the central modulatory domain of the IP_3R. Moreover, Lys17, located in the BH4 domain of Bcl-2, seemed important for its binding to the IP_3R and for regulating IP_3R-mediated Ca^{2+} release. Lys17 corresponds to Asp11 in the BH4 domain of Bcl-XL and this divergence underlies a striking functional difference between the BH4-domain biology of Bcl-2 and Bcl-XL in inhibiting IP_3R channels and subsequent Ca^{2+} signaling (Monaco et al., 2012b). Sequence analysis of this Bcl-2-binding site on the IP_3R revealed a significant resemblance to a highly conserved stretch of 22 amino acids present in the ryanodine receptor (RyR) channels, the other major class of tetrameric intracellular Ca^{2+}-release channels (Lanner et al., 2010).

Guided by this remarkable sequence similarity, we now show that Bcl-2, through its BH4 domain, directly targets RyR channels in both ectopic expression systems and native rat hippocampi, thereby inhibiting RyR-mediated Ca^{2+} release in RyR-expressing cell models as well as in hippocampal neurons.

RESULTS

Bcl-2 interacts with RyR channels in HEK293 cell models and in rat hippocampal brain lysates

The Bcl-2-binding site located in the central modulatory domain of the IP_3R (amino acids 1389–1408 for mouse IP_3R1) is well characterized (Rong et al., 2008). This binding site shows great

[1]KU Leuven, Laboratory of Molecular and Cellular Signaling, Department of Cellular and Molecular Medicine, B-3000 Leuven, Belgium. [2]University of Ghent, Physiology Group, Department Basic Medical Sciences, B-9000 Ghent, Belgium. [3]Institut de Neurobiologie Alfred Fessard, CNRS, Laboratoire de Neurobiologie et Développement, 91198 Gif sur Yvette cedex, France. [4]University of Siena, Molecular Medicine Section, Department of Molecular and Developmental Medicine, and Interuniversitary Institute of Myology, 53100 Siena, Italy. [5]Radboud University Medical Center, Donders Institute for Brain, Cognition and Behaviour, Department of Cognitive Neuroscience, 6500HB Nijmegen, The Netherlands.

*Author for correspondence (geert.bultynck@med.kuleuven.be)

Received 17 January 2014; Accepted 7 April 2014

Journal of Cell Science

Journal of Cell Science (2014) 127, 2782–2792 doi:10.1242/jcs.150011

similarity with a region located in the central part of the RyR (amino acids 2448–2469 for rabbit RyR1). Given that IP_3Rs and RyRs share several binding partners important for their regulation, it was plausible that Bcl-2 also affects RyR function. In order to verify this, a co-immunoprecipitation approach in HEK293 cells stably overexpressing either RyR1 or RyR3 (HEK RyR1 and HEK RyR3, respectively) was first set up. In these clonal cell lines, RyR levels and endogenous Bcl-2 expression were assessed (Fig. 1A). RyR1 protein expression levels were lower compared to RyR3 in their respective cell lines. The RyR antibody also detected a stable breakdown product of RyR1 and RyR3, resulting in a double signal in the RyR-stained immunoblot, as described previously (Xiao et al., 2002). Interestingly, overexpressing either RyR1 or RyR3, respectively, induced a 2.36±0.30- and 2.77±0.45-fold (mean±s.d.) increase of endogenous Bcl-2 protein levels in comparison to the HEK cells stably expressing the empty vector (HEK mock). Immunoprecipitation of either RyR3 from HEK RyR3 cells (Fig. 1B) or RyR1 from HEK RyR1 cells (Fig. 1C) resulted in the co-immunoprecipitation of endogenous Bcl-2 (lanes 1 and 2) as well as of transiently overexpressed 3×FLAG–Bcl-2 (lanes 3 and 4). We have previously described that the Bcl-2^{K17D} mutant displayed much weaker binding to the regulatory domain of the IP_3R than does wild-type Bcl-2 (Monaco et al., 2012b). However, 3×FLAG–Bcl-2^{K17D} still co-immunoprecipitated with both RyR3 and RyR1 proteins (Fig. 1D,E). Next, we examined whether endogenous RyR–Bcl-2 complexes were present *in vivo*. Hence, lysates from rat hippocampi, which express all three known RyR isoforms, with RyR2 being the most abundantly expressed isoform (Martin et al., 1998; Sharp et al., 1993), were prepared. In these lysates, Bcl-2 co-immunoprecipitated with the endogenous RyRs using the pan-RyR antibody, indicating the presence of endogenous RyR–Bcl-2-protein complexes (Fig. 1F).

Bcl-2 targets the central domain of the different RyR isoforms through its BH4 domain

The above experiments established that Bcl-2 is found in RyR-containing protein complexes, but neither clarified whether Bcl-2 directly binds to RyR channels nor identified the molecular determinants underlying this interaction. Therefore, we exploited previously gained insights into the domains of IP_3Rs and Bcl-2 responsible for IP_3R–Bcl-2-complex formation (Monaco et al., 2012a; Monaco et al., 2012b; Rong et al., 2009). Fig. 2A shows the sequence comparison between the different IP_3R and RyR isoforms, focusing on the known Bcl-2-binding site on the IP_3Rs (Rong et al., 2008). RyR protein domains covering ~400 amino acids of the central region and containing the putative Bcl-2-binding site on RyR1, RyR2 and RyR3 [amino acids 2404–2827

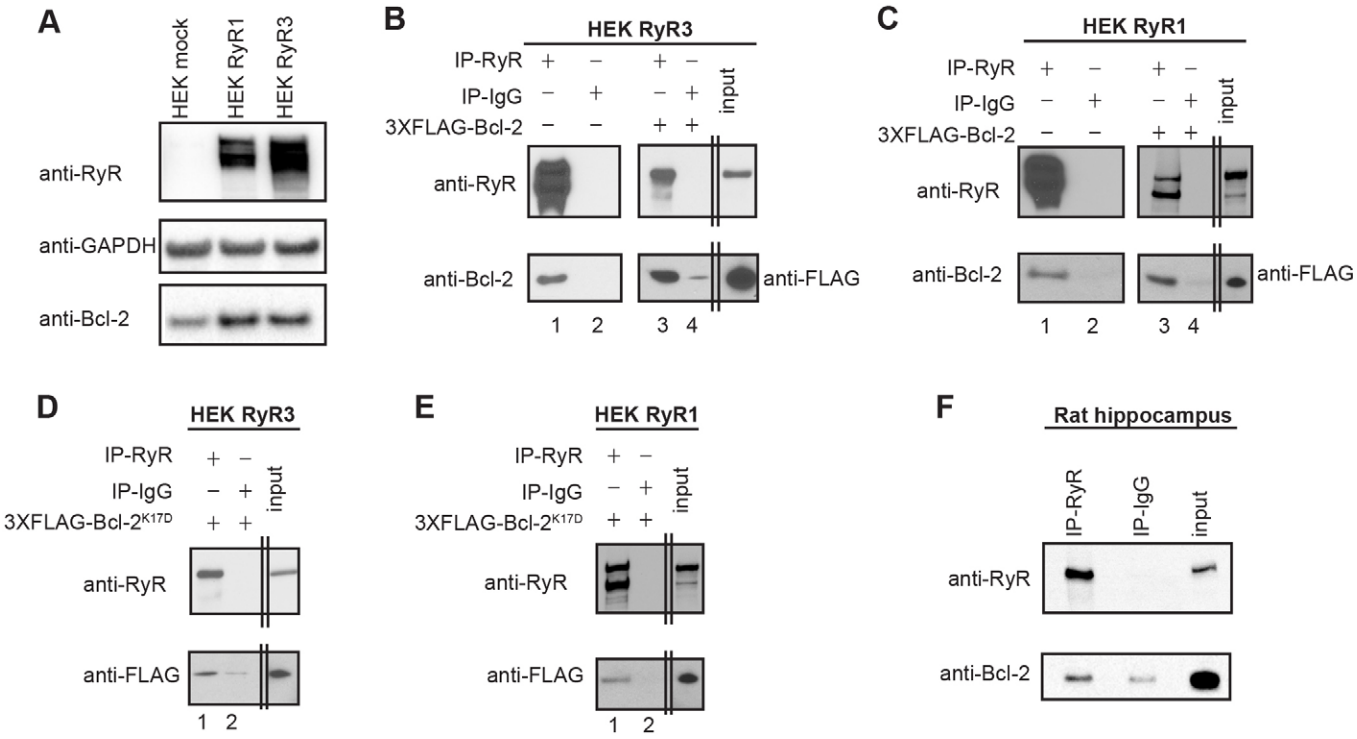

Fig. 1. Bcl-2 interacts with both overexpressed and endogenous RyRs. (A) Immunoblot showing the expression of RyRs, Bcl-2 and GAPDH (loading control) in cell lysates from empty-vector-expressing HEK cells (HEK mock), RyR1-expressing HEK cells (HEK RyR1) and RyR3-expressing HEK cells (HEK RyR3). (B,C) Immunoblots from co-immunoprecipitation experiments using HEK RyR3 (B) and HEK RyR1 (C) cell lysates. RyR3 or RyR1 was immunoprecipitated using a pan-RyR antibody. Co-immunoprecipitation of endogenous Bcl-2 with RyRs (lanes 1 and 2) was assessed by immunoblotting using a Bcl-2 antibody. Co-immunoprecipitation of ectopically expressed 3×FLAG–Bcl-2 (lanes 3 and 4) was assessed by immunoblotting using a FLAG antibody. (D,E) Lanes 1 and 2 show similar experiments performed as in B and C (lanes 3 and 4), but utilizing the 3×FLAG–Bcl-2^{K17D} mutant. Immunoprecipitations using non-specific IgGs were included for every condition to assess the level of non-specific binding. 0.2 and 0.5 µg of total cell lysate was taken as input for the 3×FLAG-tagged proteins and the RyR, respectively (input). (F) Immunoblots showing a typical co-immunoprecipitation experiment using lysates obtained from 21-day-old rat hippocampi. The endogenous RyRs were immunoprecipitated and the presence of endogenous Bcl-2–RyR complexes was assessed using a Bcl-2 antibody. The IgG co-immunoprecipitation was used as negative control. 10 µg of total lysates was used as input. Each experiment was performed at least three times utilizing each time a newly prepared cell or hippocampal lysate. The double lines in panel B to E indicate where two parts of the same immunoblot (taken with the same exposure time) were merged.

Journal of Cell Science (2014) 127, 2782–2792 doi:10.1242/jcs.150011

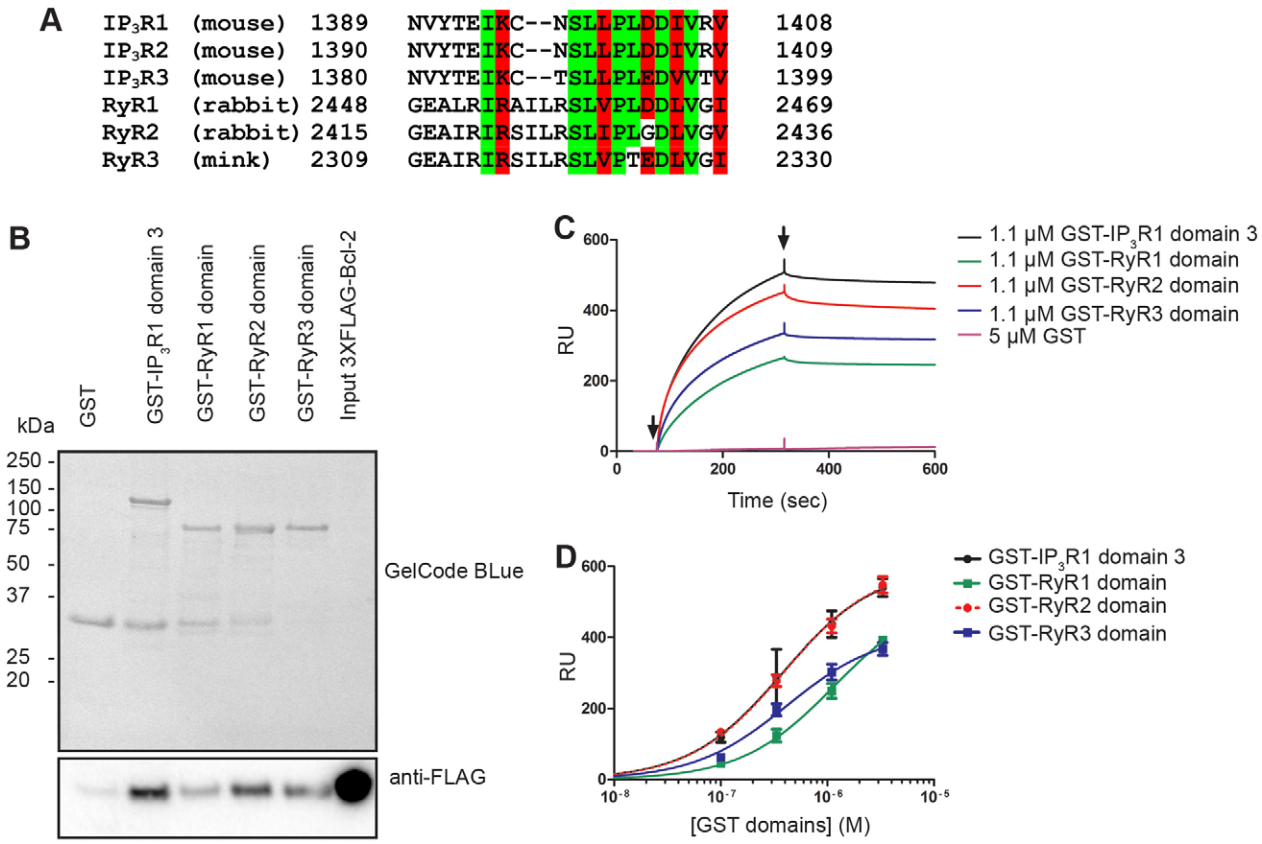

Fig. 2. Bcl-2 binds to RyRs through its BH4 domain. (A) Sequence alignment of the relevant sites on the three mouse IP_3R isoforms (IP_3R1, amino acids 1389–1408; IP_3R2, amino acids 1390–1409; IP_3R3, amino acids 1380–1499) and the three RyR isoforms (rabbit RyR1, amino acids 2448–2469; rabbit RyR2, amino acids 2415–2436; mink RyR3, amino acids 2309–2330) based on the known Bcl-2-binding site on the IP_3R. Identical (green) or similar (red) amino acids are indicated. (B) Example of the performed GST pulldown experiments. Top: GelCode Blue staining of an immunoblot showing total amounts of the pulled-down GST or GST-tagged proteins. Bottom: immunoblot stained with FLAG antibody showing the amounts of pulled-down 3×FLAG-Bcl-2 protein. GST was used as a negative control. 0.1 μg of total COS-1 lysates was used as input. The experiments were repeated at least five times using at least three different batches of the GST-tagged domains and a new COS-1 cell lysate each time. (C) Representative, background-corrected sensorgrams obtained from SPR experiments in which biotin–BH4-Bcl-2 immobilized to streptavidin-coated sensor chips was exposed to GST-tagged proteins (1.1 μM) or GST alone (5 μM). Binding is expressed in resonance units (RU) as a function of time. Binding of the GST fusion proteins to the biotin–BH4-Bcl-2 was corrected for non-specific binding by subtracting the response of these proteins to the biotin-scrambled BH4 domain loaded in a different channel on the same sensor chip. The first arrow indicates the start of the association phase (addition of the GST fusion proteins or GST diluted in running buffer); the second arrow indicates the start of the dissociation phase (running buffer alone). All experiments were performed using different sensor chips and at least three different preparations of the GST-tagged proteins. (D) Averages of the responses to the GST-tagged proteins for each tested concentration were determined and used to fit dose–response curves. For clarity reasons, the fitted curve corresponding to the RyR2 domain is depicted here as a dashed line. Data points indicate mean±s.e.m. (n=3).

for RyR1 (rabbit), 2369–2794 for RyR2 (rabbit) and 2263–2688 for RyR3 (mink)] were cloned, expressed and purified as recombinant GST fusion proteins. The different purified GST–RyR domains were used in GST pulldown assays in combination with cell lysates from COS-1 cells transiently overexpressing 3×FLAG–Bcl-2 (Fig. 2B). The previously characterized domain 3 of the IP_3R1 was used as a positive control (Rong et al., 2008). 3×FLAG–Bcl-2 was pulled down by the IP_3R1 domain as well as by the different RyR domains (Fig. 2B). The binding of 3×FLAG–Bcl-2 to the purified GST–RyR domains was consistently higher than its binding to GST (supplementary material Fig. S1). These data suggest that Bcl-2 interacts with all three RyR isoforms through a binding site that is located in the central domain of the RyRs.

To assess whether Bcl-2 is able to directly bind to the purified RyR domains and clarify whether this binding occurs through the BH4 domain of Bcl-2, we performed surface plasmon resonance (SPR) experiments. In addition, these data allow for a more quantitative assessment of the RyR–Bcl-2 interaction. In these experiments, the binding of the purified GST–RyR domains to a biotinylated version of the BH4 domain of Bcl-2 was monitored. All signals were corrected for background binding to a biotinylated scrambled BH4 peptide immobilized to another channel on the same chip. Purified GST–IP_3R1 domain 3 (the positive control) and the respective GST–RyR domains were used as analytes. A concentration-dependent increase in resonance units (RU) indicated a specific binding to biotin–BH4-Bcl-2 for the GST–IP_3R1 domain 3 as well as for the various GST–RyR domains (Fig. 2C,D). Purified GST did not show any substantial binding to the BH4 domain of Bcl-2 (Fig. 2C). In all cases, the dissociation of the IP_3R and RyR domains from biotin–BH4-Bcl-2 was very slow. Fitted concentration–response curves (Fig. 2D) were determined and used to obtain approximated EC_{50} values (Table 1). The EC_{50} value for GST–IP_3R1 domain 3 (0.38 μM) was very similar to those obtained for the GST–RyR2 domain (0.38 μM) and

Journal of Cell Science (2014) 127, 2782–2792 doi:10.1242/jcs.150011

Table 1. Affinity of biotin–BH4-Bcl-2 and biotin–BH4-Bcl-2^{K17D} for the used GST-tagged IP$_3$R1 and RyR domains

	Approximate EC_{50} values (μM)	
	BH4	BH4^{K17D}
RyR1 domain	1.53	1.61
RyR2 domain	0.38	0.80
RyR3 domain	0.37	0.78
IP$_3$R1 domain 3	0.38	1.87

Approximated EC_{50} values obtained from fitting using the Hill equation of the data presented in Fig. 3.

GST–RyR3 domain (0.37 μM). Only the binding of the GST–RyR1 domain seemed to display a lower affinity (EC_{50} value of 1.53 μM). This indicates that the BH4 domain of Bcl-2 binds to the RyR2 and RyR3 with nearly similar affinities to that of IP$_3$R1, whereas the affinity of Bcl-2 binding to RyR1 is lower. Given that the binding of Bcl-2 to GST–IP$_3$R1 domain 3 is dependent on the presence of Lys17, we also monitored the binding of the different GST–RyR domains to the biotin–BH4-Bcl-2^{K17D} mutant. The binding of wild-type BH4-Bcl-2 and BH4-Bcl-2^{K17D} to each GST fusion protein were compared (Fig. 3) and the obtained EC_{50} values are presented in Table 1. In agreement with our previous findings (Monaco et al., 2012b), binding of the GST–IP$_3$R1 domain to biotin–BH4-Bcl-2^{K17D} was severely compromised in comparison to binding of biotin–BH4-Bcl-2. In contrast, the binding of the GST–RyR domains was either not affected (in the case of RyR1) or only slightly affected (in the case of RyR2 and RyR3).

Collectively, these data indicate that Bcl-2, through its BH4 domain, directly binds to a central region in all three RyR isoforms. Although the BH4 domain was found to be responsible for binding to both the RyR and the IP$_3$R, the molecular determinants for binding to the RyR were not identical to those for binding to IP$_3$Rs.

Bcl-2 overexpression inhibits RyR-mediated Ca^{2+} release

We next set out to identify possible functional effects of the Bcl-2–RyR interaction. We performed single-cell [Ca^{2+}] measurements to assess the ability of full-size Bcl-2 to inhibit RyR-mediated Ca^{2+} release in a cellular environment. The empty pCMV24 vector, a 3×FLAG–Bcl-2 or a 3×FLAG–Bcl-2^{K17D}-containing vector was co-transfected with an mCherry-expressing plasmid in HEK RyR3 cells. Fura-2-AM was used as a cytosolic Ca^{2+} indicator in mCherry-positive cells. All these [Ca^{2+}] measurements were performed in the presence of an extracellular Ca^{2+} chelator (BAPTA) in order to study intracellular Ca^{2+}-release events. Caffeine concentrations (1.5 mM) generating sub-maximal responses in these cells were used to induce RyR-mediated Ca^{2+} releases. A typical experiment showing averaged calibrated single-cell [Ca^{2+}] traces of Fura-2-loaded HEK RyR3 cells expressing the empty vector, 3×FLAG–Bcl-2 or 3×FLAG–Bcl-2^{K17D} is shown in Fig. 4A. Overall, overexpression of 3×FLAG–Bcl-2 or 3×FLAG–Bcl-2^{K17D} inhibited the caffeine-induced Ca^{2+} release by ~30% compared to the empty-vector control (Fig. 4B). The ER Ca^{2+}-store content was measured by blocking SERCA using 1 μM thapsigargin in the presence of extracellular BAPTA and assessing the total amount of Ca^{2+} released from the stores (area under the curve). These results are summarized in Fig. 4C and indicate that overexpression of 3×FLAG–Bcl-2 or 3×FLAG–Bcl-2^{K17D} did not significantly affect the ER Ca^{2+}-store content in these cells. Similar findings were obtained by overexpressing Bcl-2 or the Bcl-2^{K17D} mutant in HEK RyR1 cells (supplementary material Fig. S2). Because RyR1 expression levels were slightly lower compared to RyR3 (Fig. 1A) and it was previously reported that, in contrast to the HEK RyR3 cells, these HEK RyR1 cells are less sensitive to stimulation with caffeine (Rossi et al., 2002), a higher concentration of caffeine (4.5 mM) was used to obtain adequate sub-maximal responses.

To verify whether the caffeine-induced Ca^{2+} release was dependent on the RyR, similar experiments were also performed

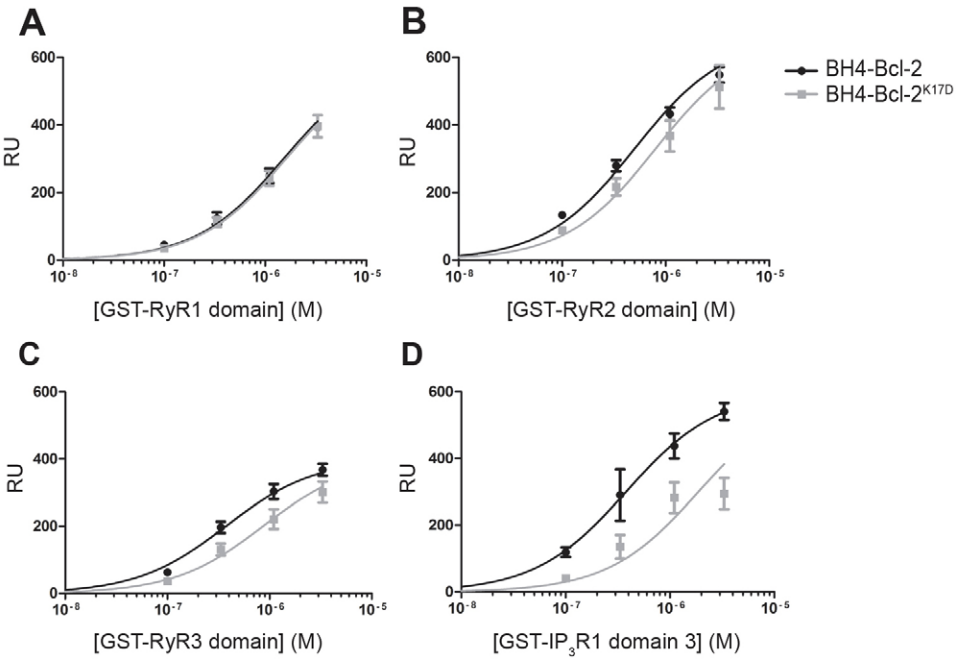

Fig. 3. Comparison of biotin–BH4-Bcl-2 and biotin–BH4-Bcl-2^{K17D} for binding to the GST-RyR domains. Binding of the different GST domains to biotin–BH4-Bcl-2 and biotin–BH4-Bcl-2^{K17D} was compared in SPR experiments similarly performed to Fig. 2C,D. Biotin–BH4-Bcl-2^{K17D} was immobilized to a different channel on the same sensor chip as biotin–BH4-Bcl-2. Averages of the responses to the GST-tagged proteins for each concentration were determined and plotted for both the wild-type BH4-Bcl-2 and the BH4-Bcl-2^{K17D} mutant. Data points indicate mean±s.e.m. (n=3). Estimated EC_{50} values obtained from the fitted dose response–curves are shown in Table 1.

Journal of Cell Science (2014) 127, 2782–2792 doi:10.1242/jcs.150011

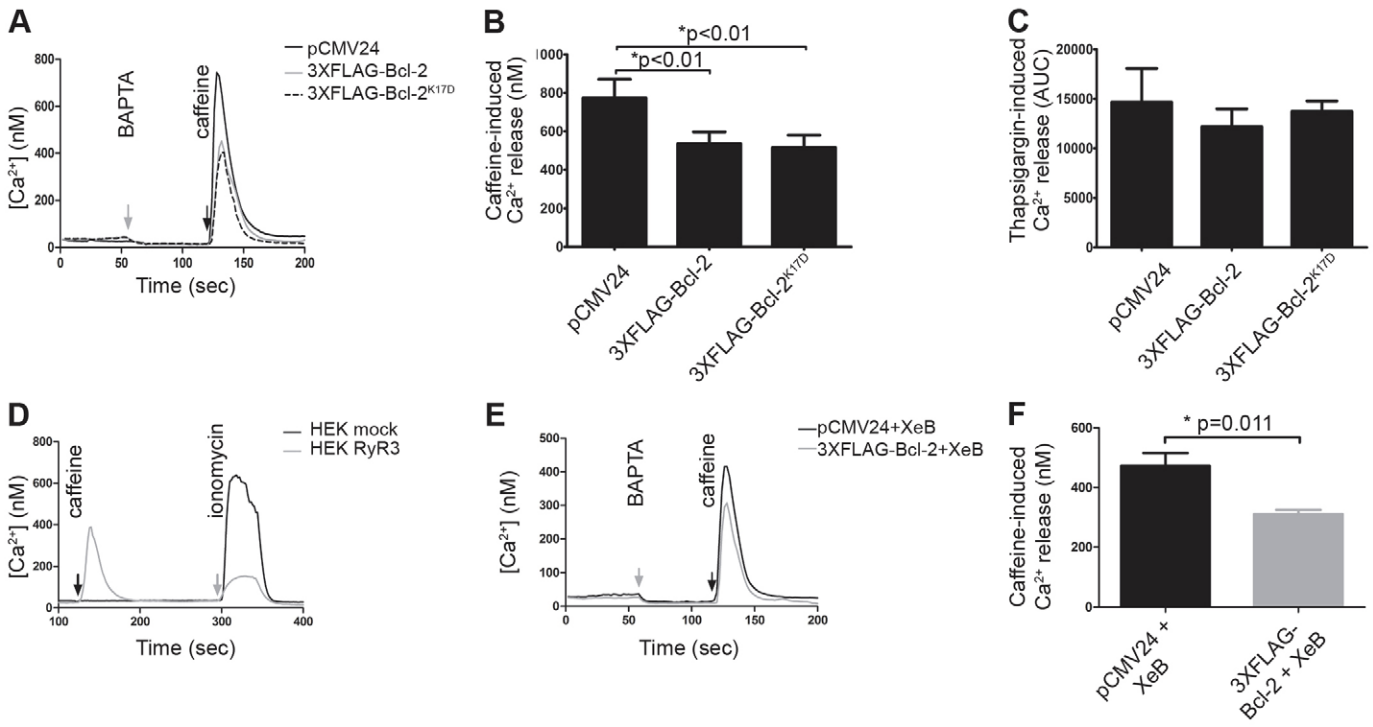

Fig. 4. Overexpression of Bcl-2 inhibits RyR-mediated Ca^{2+} release. Fura-2-loaded transfected (mCherry-positive) HEK RYR3 cells were selected for single-cell [Ca^{2+}] measurements. (A) Mean calibrated [Ca^{2+}] traces (20 cells) from HEK RyR3 cells containing the pCMV24 vector, 3×FLAG–Bcl-2 or 3×FLAG-Bcl-2^{K17D} obtained in one experiment. The administration of BAPTA (3 mM) and caffeine (1.5 mM) is indicated by the arrows. (B) Quantitative analysis of the caffeine responses in HEK RyR3 cells; values show mean±s.e.m. of at least four independent experiments (n>100 cells). (C) Quantitative analysis of the ER Ca^{2+}-store content. The ER Ca^{2+}-store content was determined similarly to A, except that thapsigargin (1 μM) was used instead of caffeine. The area under the curve (AUC) of the calibrated traces was used for determining the total ER Ca^{2+}-store content. The bar graph indicates the mean AUC (±s.e.m.) of at least three independent experiments (n>80 cells) for each condition. (D) Average calibrated [Ca^{2+}] traces (20 cells) from HEK mock or HEK RyR3 cells. The administration of caffeine (1.5 mM) and ionomycin (2 μM) is indicated by the arrows. (E) Typical experiment depicting mean calibrated [Ca^{2+}] traces (20 cells) from empty-vector control cells and 3×FLAG–Bcl-2-expressing cells showing caffeine-induced Ca^{2+} release in the presence of 2 μM of the IP_3R inhibitor XeB. The administration of BAPTA (3 mM) and caffeine (1.5 mM) is indicated by the arrows. (F) Quantification of the caffeine responses for each condition in the presence of XeB. Values depict mean±s.e.m. of at least five independent experiments (n>80 cells per condition).

using HEK mock cells lacking RyRs. In contrast to the HEK RyR3 cells, administering caffeine did not generate a Ca^{2+} response in HEK mock cells (Fig. 4D). Addition of 2 μM ionomycin resulted, however, in a rise in cytosolic [Ca^{2+}] in both cell lines, showing that the lack of a caffeine response in HEK mock cells was due to the absence of RyRs. The ionomycin response was lower in the HEK RyR3 cells owing to a partial depletion of the ER Ca^{2+} pool generated by the caffeine response prior to the addition of ionomycin.

Given that Bcl-2 is known to inhibit IP_3Rs and Ca^{2+} release from IP_3Rs can activate RyRs via Ca^{2+}-induced Ca^{2+} release, we wanted to exclude that Bcl-2's inhibitory effect on the caffeine-induced Ca^{2+} release occurred via an indirect effect on the IP_3R. To completely exclude this possibility, [Ca^{2+}] measurements were performed in HEK RyR3 cells in the presence of 2 μM xestospongin B (XeB), an IP_3R inhibitor (Jaimovich et al., 2005). Overexpression of 3×FLAG–Bcl-2 remained equally potent in inhibiting caffeine-induced Ca^{2+} release in RyR3-expressing HEK cells in the presence of XeB (and thus absence of IP_3R activity) (Fig. 4E,F). Given that Bcl-2 inhibits RyR-mediated Ca^{2+} release in the presence of a pharmacological IP_3R inhibitor and because the Bcl-2^{K17D} mutant is equally potent in inhibiting RyR-mediated Ca^{2+} release as wild-type Bcl-2, we postulate that the Bcl-2-mediated inhibition of caffeine-induced Ca^{2+} release is due to an inhibition of the RyRs and is not a result of inhibition of IP_3Rs or altered ER store content.

The BH4 domain of Bcl-2 is sufficient to inhibit RyR-mediated Ca^{2+} release in HEK RyR3 cells

The single-cell [Ca^{2+}] measurements indicated that the RyR–Bcl-2 interaction inhibits RyR-mediated Ca^{2+} release. In addition, the SPR data (Fig. 2) showed that the Bcl-2–RyR interaction occurs at least in part through the BH4 domain of Bcl-2. We next wanted to identify whether the BH4 domain of Bcl-2 was sufficient to inhibit RyR channels. Hence, we measured RyR-mediated Ca^{2+} release in Fluo-3-loaded HEK RyR3 cells loaded with different concentrations of BH4-Bcl-2 peptide or a scrambled counterpart (Fig. 5A,B). Entry of the peptide into the cells was mediated by electroporation loading, as previously described (De Vuyst et al., 2008). Compared to the vehicle control, electroporation loading of the cells with BH4-Bcl-2 (20 μM) caused a prominent decrease in the caffeine-induced Ca^{2+} release. Performing the same experiment with the scrambled BH4-Bcl-2 peptide (20 μM) did not alter caffeine-induced Ca^{2+} release (Fig. 5A). Electroporation loading of increasing concentrations of BH4-Bcl-2 resulted in a concentration-dependent inhibition of the caffeine-induced Ca^{2+} release, which was not observed utilizing the scrambled BH4-Bcl-2 (Fig. 5B).

Journal of Cell Science (2014) 127, 2782–2792 doi:10.1242/jcs.150011

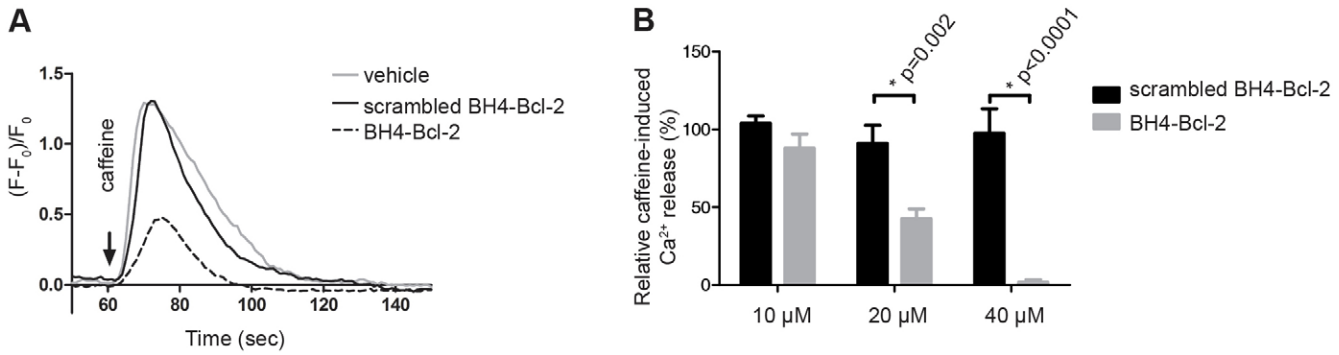

Fig. 5. The BH4 domain of Bcl-2 is sufficient for inhibiting RyR3-mediated Ca^{2+} release. Single-cell Fluo-3 [Ca^{2+}] measurements were performed in HEK RyR3 cells. The vehicle (DMSO), the BH4 domain of Bcl-2 or the scrambled peptide were loaded by electroporation (10, 20 or 40 µM), after which 1 mM of caffeine was used as stimulus. (A) Typical traces obtained for each condition after electroporation loading with 20 µM of the peptides or the vehicle. The arrow indicates the time when caffeine (1 mM) was added. The traces are represented as $(F-F_0)/F_0$. (B) Quantitative analysis of all experiments. Means of five independent experiments are given as relative responses (±s.e.m.) compared to the DMSO control. The caffeine responses were normalized to the vehicle control.

The BH4 domain of Bcl-2 inhibits RyR-mediated Ca^{2+} release in hippocampal neuronal cultures

The present data clearly show that the BH4 domain of Bcl-2 is sufficient to bind to and inhibit RyRs. Because these experiments were all performed in cellular models overexpressing RyRs, we next wanted to examine whether the BH4 domain of Bcl-2 is also able to inhibit endogenous RyR channels. Given the presence of endogenous RyR–Bcl-2 complexes in rat hippocampal neurons (Fig. 1F), we opted to study the regulation of RyR channels by the BH4 domain of Bcl-2 in these cells.

Dissociated hippocampal neurons were infected at 7 days *in vitro* (DIV) with an adeno-associated virus expressing GCaMP3. Single-cell [Ca^{2+}] measurements were performed between 14 and 18 DIV. GCaMP3 was used as a genetically encoded fluorescent Ca^{2+} indicator (Yamada and Mikoshiba, 2012). Utilizing whole-cell voltage-clamp, the membrane potential was clamped at −60 mV thereby preventing Ca^{2+} influx from the extracellular space through voltage-gated Ca^{2+} channels. In this way, the measured changes in fluorescence could be attributed to changes in intracellular Ca^{2+} release and were not due to Ca^{2+} influx across the plasma membrane. At the same time the BH4 domain of Bcl-2, the scrambled BH4-domain peptide or the vehicle control (DMSO) were introduced into the neurons by means of the patch pipette. A scheme of the experimental protocol is provided in Fig. 6A. Local application of 10 mM caffeine resulted in RyR-mediated Ca^{2+} release. Fig. 6B shows representative images from a time-lapse experiment, and Fig. 6C shows a typical trace obtained for each condition. Introducing the BH4 domain of Bcl-2 (20 µM) into the soma of the neurons led to a prominent inhibition of the caffeine-induced Ca^{2+} release compared to introducing either the vehicle (DMSO) control or the scrambled BH4 domain of Bcl-2 in the neurons (Fig. 6B–D). Pretreatment of the neurons with 50 µM ryanodine almost completely blocked caffeine-induced Ca^{2+} release, indicating that the observed Ca^{2+} release can be attributed to RyR activity (Fig. 6E). Taken together, these data indicate that the BH4 domain of Bcl-2 can inhibit native RyR channels in hippocampal neurons.

DISCUSSION

The major finding of this study is that RyR channels, an important class of intracellular Ca^{2+}-release channels, are targets for the anti-apoptotic Bcl-2 proteins in both ectopic-RyR-expressing cell systems and primary tissues, like the hippocampus. We showed that Bcl-2, through its BH4 domain, directly binds to the central domain of the RyR channels, thereby suppressing RyR-mediated Ca^{2+} release. These findings clearly underpin the emerging role for Bcl-2 proteins in intracellular Ca^{2+} signaling by directly targeting an increasing number of Ca^{2+}-transporting systems at intracellular and plasmalemmal membranes, including IP_3Rs (Hanson et al., 2008; Rong et al., 2009; Rong et al., 2008), SERCA (Kuo et al., 1998), VDAC (Arbel and Shoshan-Barmatz, 2010), BI-1 (Ahn et al., 2010; Xu and Reed, 1998) and PMCA (Ferdek et al., 2012).

The binding of Bcl-2 to the RyR shows a striking resemblance with the binding of Bcl-2 to the IP_3R. The latter is interesting because IP_3Rs and RyRs show many similarities at both the structural and functional level (Furuichi et al., 1994; Seo et al., 2012). Both intracellular Ca^{2+}-release channels are modulated by the same cellular factors, like Ca^{2+}, ATP and Mg^{2+} (Bezprozvanny et al., 1991; Bull et al., 2007; Dias et al., 2006; Maes et al., 2001; Mak and Foskett, 1998). In addition, several kinases target both channels e.g. protein kinase A (PKA), PKC, PKG and Ca^{2+}/calmodulin-dependent protein kinase II (Furuichi et al., 1994; Lanner et al., 2010; Vanderheyden et al., 2009). Different regulatory proteins interact with both the IP_3Rs and the RyRs. Calmodulin for example regulates the Ca^{2+} sensitivity of IP_3Rs (Kasri et al., 2004) and RyRs (Balshaw et al., 2001). Our data now clearly indicate that, in a similar way as for the IP_3R (Rong et al., 2008), RyRs are also targets of Bcl-2. Importantly, the RyRs contain a sequence that has ~60% similarity to the Bcl-2-binding site located in the central modulatory region of IP_3Rs (Rong et al., 2008). Bcl-2 binds to this site on the IP_3R through its BH4 domain (Rong et al., 2009). Our results (Fig. 2) indicate that Bcl-2 behaves in a similar manner with respect to the RyRs. This similarity extends to the functional level because binding of the BH4 domain of Bcl-2 leads, in both IP_3Rs (Rong et al., 2009) and RyRs, to a suppression of channel-mediated Ca^{2+} release.

Sequence alignment revealed a 22-amino-acid spanning region (amino acids 2309–2330, mink RyR3) in the RyR that displays striking similarity to the known Bcl-2-binding site of the IP_3R. In addition, the proposed region is highly conserved across all RyR isoforms of different species. It can be anticipated that regulation of RyRs by Bcl-2 is important, as the proposed Bcl-2-binding site

Journal of Cell Science (2014) 127, 2782–2792 doi:10.1242/jcs.150011

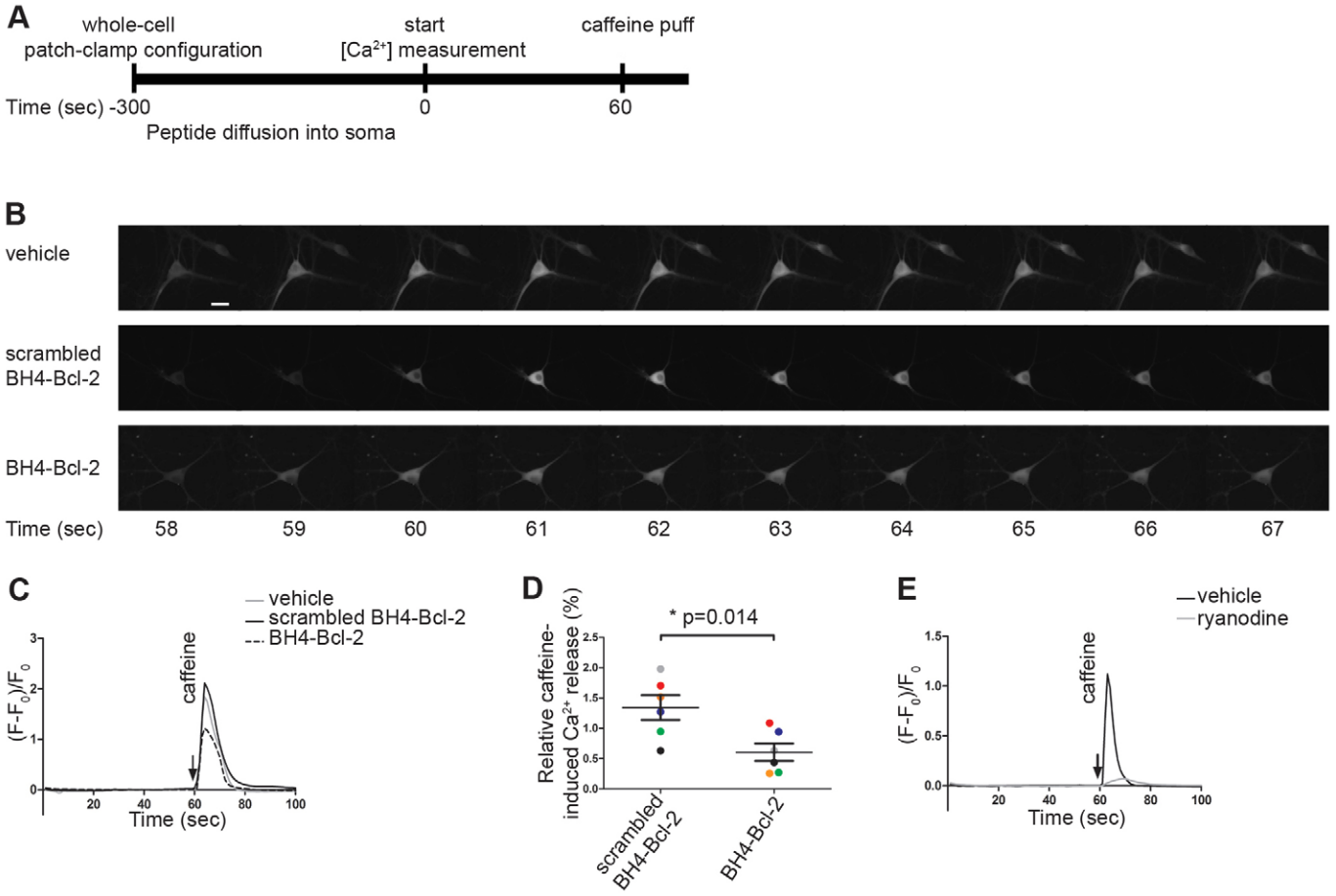

Fig. 6. The BH4 domain of Bcl-2 inhibits RyR-mediated Ca^{2+} release in hippocampal neuronal cultures. Single-cell [Ca^{2+}] measurements were performed on 14- to 18-day-old dissociated hippocampal neuronal cultures. GCaMP3-positive cells were selected for the measurements. The vehicle (DMSO), a scrambled version of the BH4 domain of Bcl-2 (20 μM) or the BH4 domain of Bcl-2 (20 μM) were introduced into the cell through the patch pipette. At the same time, the membrane potential was clamped at −60 mV. (A) Scheme of the performed experiment starting from the time when the whole-cell voltage-clamp was obtained. Caffeine (10 mM) was locally applied through a second patch pipette positioned next to the cell. (B) Time lapse of a typical experiment for each tested condition performed, focusing on the time when caffeine was applied locally. Scale bar: 5 μm. (C) Typical caffeine-induced Ca^{2+}-release responses measured in the soma of one neuron for each tested condition. The fluorescence was normalized to the baseline fluorescence and represented as $(F-F_0)/F_0$. The arrow indicates the time point when caffeine was applied. (D) Summary of all performed measurements for the scrambled BH4 domain of Bcl-2 and the BH4 domain of Bcl-2 normalized to the vehicle control. The circles indicate the average of all [Ca^{2+}] measurements (2 to 4 cells) performed per condition each day. [Ca^{2+}] measurements performed on the same day are indicated in the same color. The mean±s.e.m. of six independent experiments is indicated in black (n=19 cells for each condition). (E) Typical single-cell [Ca^{2+}] measurement performed in neurons pretreated for 20 min with either the vehicle (DMSO) (black) or 50 μM ryanodine (gray). The arrow indicates the time point when caffeine was applied. The fluorescence was normalized to the baseline fluorescence and represented as $(F-F_0)/F_0$. Experiments were performed at least five times.

on the RyR is already known to be a crucial regulatory site for RyR channel stability. Structural coupling (RyR zipping) of this centrally located site to the N-terminus is crucial for adequate RyR functioning (Ikemoto and Yamamoto, 2002; Yamamoto and Ikemoto, 2002). Disruption of this interaction (RyR unzipping) generates leaky RyR channels and triggers irregular channel activity. This central site is also part of a mutational hotspot in RyR1 and RyR2 involved in the onset of malignant hyperthermia (Hwang et al., 2012) and arrhythmia (Yano, 2008), respectively. Structural information about this mutational hotspot has been obtained from 3D cryo-EM studies. In an elegant study, a GFP tag was introduced at residue 2367 of RyR2 (Liu et al., 2005), ~60 amino acids upstream of the Bcl-2-binding site described here. The location of the GFP insert was mapped to a bridge area between domain 5 and domain 6 (Liu et al., 2005). This area is known to be located at the cytoplasmic face of the RyR (Radermacher et al., 1994). Thus, we anticipate that the region where the Bcl-2-binding site is located should be accessible for interaction.

In addition, a proposed binding site for the 12-kDa and 12.6-kDa FK506-binding proteins [FKBP12 and FKBP12.6 (also known as FKBP1A and FKBP1B, respectively)] on the different RyR isoforms is located within the binding domain for Bcl-2 on the RyRs identified in this study (Brillantes et al., 1994; Bultynck et al., 2001b; Gaburjakova et al., 2001; Marx et al., 2000; Van Acker et al., 2004). Both FKBP12 and FKBP12.6 are immunophilins that are tightly associated with the RyR and are necessary for stabilizing the channel (Brillantes et al., 1994). In this way, these proteins inhibit excessive Ca^{2+} leak through RyRs. Given that Bcl-2 targets a site in close proximity to a FKBP12- or FKBP12.6-binding site, it is not surprising that Bcl-2 binding to RyRs has functional consequences. It remains to be determined

whether the binding of immunophilins and Bcl-2 family proteins compete for the same, similar or overlapping sites, and whether RyR–Bcl-2 complexes are present in tissues containing high levels of FKBP12 and/or FKBP12.6, such as skeletal and cardiac muscle. In any case, further experiments are needed, as additional FKBP12- and/or FKBP12.6-binding sites on RyR channels have been proposed. More specifically, for the cardiac RyR2 channel, FKBP12.6 has been described to bind to both an N-terminal site (Masumiya et al., 2003) and a C-terminal site (Zissimopoulos and Lai, 2005a; Zissimopoulos and Lai, 2005b). Further experiments investigating competition between Bcl-2 and FKBP12 and/or FKBP12.6 for the binding to the different RyR isoforms might therefore provide additional insights into these apparent discrepancies. Furthermore, we previously reported that despite sequence similarities between the proposed FKBP12-binding site on IP_3Rs and RyRs, their properties and secondary structure might be different (Bultynck et al., 2001a; Bultynck et al., 2001b). Hence, these differences might contribute to the fact that in IP_3Rs this site preferentially binds Bcl-2 over the Bcl-2^{K17D} mutant, whereas for the equivalent site in the RyRs there was a nearly similar binding of Bcl-2 and Bcl-2^{K17D}. Finally, other factors, such as ATP, might also influence Bcl-2 binding to the RyR as the proposed site for Bcl-2 binding in RyRs has also been implicated in ATP binding (Blayney et al., 2013; Zissimopoulos and Lai, 2005b).

The role of RyRs in cell survival and cell death decisions is much less well documented than for the IP_3R. RyRs, however, can, similar to IP_3Rs, also mediate Ca^{2+} signaling into mitochondria (Hajnóczky et al., 2002). The exact molecular mechanisms of this Ca^{2+} transfer to the mitochondria remain poorly understood. A recent paper has shown that VDAC2 is coupled to RyR2 in the heart (Min et al., 2012), allowing a direct coupling of RyR-mediated Ca^{2+} release to Ca^{2+} uptake in the mitochondria. Moreover, RyR-mediated Ca^{2+} signaling has been implicated in ATP production and metabolic flexibility in the heart (Bround et al., 2013). Other studies have implicated RyRs in the regulation of apoptosis (Kim et al., 2002) and ER-stress-mediated cell death (Luciani et al., 2009; Ruiz et al., 2009) in various cell types, including neurons and pancreatic β cells. The Bcl-2–RyR interaction described here could therefore provide an important regulatory mechanism by which RyR activity controls cell fate. Further studies will be needed to unravel the exact cell biological and/or physiological role of Bcl-2 binding to RyRs in cell fate decisions and functions beyond apoptosis. It is becoming increasingly clear that Ca^{2+} signaling and RyRs play important roles in memory formation and neurodegenerative diseases (Berridge, 2013; Berridge, 2011). The presence of RyR–Bcl-2 complexes in the hippocampus (Fig. 1F) and the observation that the BH4 domain of Bcl-2 is able to inhibit RyR-mediated Ca^{2+} release in hippocampal neurons (Fig. 6) might suggest that Bcl-2, through regulating RyR channels, has an important function in the brain.

In conclusion, we identified RyR channels as new cellular targets for anti-apoptotic Bcl-2 proteins. Our findings show that Bcl-2 targets and regulates the two main families of intracellular Ca^{2+}-release channels, IP_3Rs and RyRs, in a similar way. This further strengthens the role of Bcl-2 proteins as essential regulators of Ca^{2+}-signaling events and places RyR channels in the growing list of Ca^{2+} transport systems that are targeted by Bcl-2.

MATERIALS AND METHODS

Chemicals, antibodies and peptides

Unless otherwise specified, all chemicals were purchased from Sigma-Aldrich (St Louis, MO). XeB was isolated from *Xestospongia exigua* as previously described (Quirion et al., 1992). Mouse monoclonal anti-FLAG M2 antibody (1:3000; Sigma-Aldrich), mouse monoclonal anti-GAPDH antibody (GAPDH-71.1) (1:50000) (Sigma-Aldrich), mouse monoclonal anti-RyR antibody (34C; 1:1000; Thermo Scientific, Rockford, IL) and rabbit monoclonal anti-Bcl-2 antibody (50E3; 1:1000; Cell Signaling Technology, Boston, MA) were used throughout this study. The sequences of the peptides used in this study were: biotin–BH4-Bcl-2, biotin–RTGYDNREIVMKYIHYKLSQRGYEW; biotin–BH4-Bcl-2^{K17D}, biotin-RTGYDNREIVMDYIHYKLSQRGYEW; Biotin-scrambled BH4-Bcl-2, biotin–WYEKQRSLHGIMYYVIEDRNTKGYR. These peptides were synthesized by Life Tein (Hillsborough, NJ). The BH4-Bcl-2 and scrambled BH4-Bcl-2 peptides were also obtained without a biotin tag.

Plasmids and constructs

3×FLAG–Bcl-2 and 3×FLAG–Bcl-2^{K17D} were obtained as described previously (Monaco et al., 2012b). The rabbit RyR1 (7212–8481), RyR2 (7107–8382) and mink RyR3 (6789–8064) GST-tagged constructs were developed using previously described methods for cloning (Monaco et al., 2012b), utilizing the *Bam*HI and *Eco*RI restriction enzymes and the following primer sets: RyR1 forward, 5′-GCGGCGGGATCCCACT-TTGGGGAGGAGCCCCCTG-3′ and reverse, 5′-GCGGCGGAAT-TCCTACCTGGCCTTCTCGATCGTCC-3′; RyR2, forward, 5′-GCG-GCGGGATCCAGCAAAACACTTGATACGGAGGAG-3′ and reverse, 5′-GCGGCGGAATTCCTATCGGGTTCTTTCAATCCTCC-3′; RyR3 forward, 5′-GCGGCGGGATCCAAGAGAGAAGTCATGGAGGAC-GG-3′ and reverse, 5′-GCGGCGGAATTCCTATTTGGTCCTCTCCA-CAGACC-3′.

Protein purification

GST fusion protein purification was performed as described previously (Bultynck et al., 2001b) except for the induction of protein synthesis, which was performed with 0.1 mM isopropyl β-d-thiogalactoside for 20 h at 14℃. After the purification, dialysis and handling of the proteins was performed as described previously (Monaco et al., 2012b).

Cell culture and transfections

All media and supplements added to the medium used in this paper were purchased from Life Technologies (Ghent, Belgium). HEK293 cells stably expressing an empty pcDNA3.1(-) vector (HEK mock) or stably overexpressing RyR1 or RyR3 (Rossi et al., 2002) were cultured at 37℃ in a 5% CO_2 incubator in α-minimum essential medium supplemented with 10% fetal calf serum, 100 IU/ml penicillin, 100 µg/ml streptomycin, 2 mM glutamax and 800 µg/ml G418. COS-1 cells were cultured in Dulbecco's Modified Eagle's medium (DMEM), containing 10% fetal calf serum, 100 IU/ml penicillin, 100 µg/ml streptomycin, 2.5 µg/ml fungizone and 2 mM glutamax at 37℃ under 10% CO_2.

At 1 day after seeding, cells were transiently transfected with either empty p3XFLAG-Myc-CMV-24 or with the same vector containing Bcl-2 or Bcl-2^{K17D}. JETprime transfection reagent (Polyplus Transfections, Illkirch, France) was used according to the manufacturer's instruction. After 2 days, HEK mock, HEK RyR1 or HEK RyR3 cells were harvested and lysed using a CHAPS-based lysis buffer [50 mM Tris-HCl pH 7.5, 100 mM NaCl, 2 mM EDTA, 50 mM NaF, 1 mM Na_3VO_4, 1% CHAPS and protease inhibitor tablets (Roche, Basel, Switzerland)]. For COS-1 cells a Triton-X-100-based lysis buffer (25 mM HEPES pH 7.5, 100 mM NaCl, 1.5 mM $MgCl_2$, 0.5 mM DTT, 10% glycerol, 1% Triton X-100 and protease inhibitor tablets) was used. Cells for [Ca^{2+}] measurements were seeded in two-chamber slides and transfected 2 days later using the X-tremeGENE HP DNA transfection reagent (Roche) according to the manufacturer's protocol. As a selection marker pcDNA 3.1(-) mCherry vector was co-transfected at a 1:3 ratio to the p3XFLAG-Myc-CMV-24 vectors.

Dissociated hippocampal cultures

Dissociated hippocampal neurons were prepared as described previously (Nadif Kasri et al., 2011). Briefly, embryonic day 18 rat hippocampi were dissected and washed with ice-cold Hanks' balanced salt solution (HBSS) without Mg^{2+} or Ca^{2+} (Life Technologies) supplemented with 10 mM

HEPES at pH 7.3. Following a 15-min incubation with 0.25% trypsin at 37℃, the hippocampi were again washed with the HBSS solution. After removing the last wash, seeding medium (neurobasal medium containing 10% FBS, 100 IU/ml penicillin, 100 µg/ml streptomycin and 2% B27 supplement) was added. Using polished Pasteur pipettes the hippocampi were dissociated and seeded on polyethylene-treated coverslips at 50,000 cells per coverslip. After 4 h, half of the seeding medium was replaced with culturing medium (neurobasal medium containing 2 mM glutamax, 100 IU/ml penicillin, 100 µg/ml streptomycin and 2% B27 supplement). Half of the medium was replaced with culturing medium every 3 days. All animal experiments were performed according to approved guidelines.

GST pulldown

The purified GST fusion proteins or parental GST (0.5 µM) were incubated in the Triton X-100 lysis buffer together with 70 µg of COS-1-cell lysates overexpressing the 3×FLAG–Bcl-2 protein (final volume 500 µl). The incubation was performed at 4℃ using a head-over-head rotator. After 1 h, the GST fusion proteins were immobilized to glutathione-Sepharose® 4B beads (GE Healthcare, Diegem, Belgium). At 1.5 to 2 h later, the Sepharose beads were washed five times using Triton X-100 lysis buffer. Subsequently, the complexes were eluted in 40 µl 2×LDS (Life Technologies) supplemented with 1:200 β-mercaptoethanol for 5 min at 95℃. A total of 10 µl of the collected eluate was used for immunoblot analysis. GelCode Blue (Thermo Scientific) was used to determine the total amount of protein present on the PVDF membrane (Millipore, Billerica, MA, USA). For quantification, the amount of 3×FLAG–Bcl-2 bound to the different GST fusion proteins was divided by the amount of GST-tagged protein present on the membrane corrected for their difference in molecular mass. Values are presented relative to the amount bound to the positive control (GST-tagged IP_3R1 domain 3).

SPR analysis

SPR analysis was performed using a Biacore T100 (GE Healthcare). Immobilization to the streptavidin-coated sensor chip (BR-1005-31; GE Healthcare) and SPR measurements were performed as described previously (Monaco et al., 2012b). NaOH (50 mM) with 0.0026% SDS was used as a regeneration buffer. Dose–response curves were fitted using the Hill equation. For comparing the binding of the GST-tagged domains to the wild-type BH4-Bcl-2 and the BH4-Bcl-2^{K17D} mutant, the V_{max} of the fitted curves was fixed to the estimated value for the wild-type BH4 domain for each GST fusion domain.

Co-immunoprecipitation experiments

A co-immunoprecipitation kit (Thermo Scientific) was used. A total of 5 µg of either the RyR antibody or a mouse IgG control antibody was covalently immobilized to 20 µl of the resin according to the manufacturers' protocol except for the final washing step, which was performed using the CHAPS-based lysis buffer. Next, when using lysates of cells overexpressing RyRs and 3×FLAG–Bcl-2 proteins, 200 µg of pre-cleared cell lysate was incubated overnight at 4℃ in CHAPS lysis buffer together with the resin containing the antibody. For detection of interactions with endogenous Bcl-2 in the RyR-overexpressing HEK cells, 400 µg of cell lysate was used without prior pre-clearing. The next day, the resin was washed four or five times with CHAPS lysis buffer, after which the elution was performed by boiling the samples for 5 min at 95℃ in 50 µl of 2×LDS supplemented with 1:200 β-mercaptoethanol. 21-day-old rat hippocampi were homogenized in the CHAPS lysis buffer and incubated for 30 min at 4℃. After centrifugation (4000 ***g***) the supernatant was used for co-immunoprecipitation of endogenous Bcl-2–RyR complexes. The same protocol was used as for the co-immunoprecipitations in the HEK RyR cells with endogenous Bcl-2 with the exception that, the amount of washes was reduced to two.

Immunoblot analysis

Samples were prepared and used as previously described (Monaco et al., 2012b). For visualization of RyRs, NuPAGE 3–8% Tris acetate gels were run. Detection was performed using Pierce ECL Western Blotting Substrate (Thermo Scientific). For developing, CL-Xposure Films (Thermo Scientific) were used in combination with either an X-OMAT 1000 processor (Kodak, Zaventem, Belgium) or a Chemidoc™ MP system (Bio Rad, Nazareth Eke, Belgium).

Electroporation loading and Ca^{2+} imaging

HEK RyR3 cells were grown as adherent monolayers to near confluency on 18-mm-diameter glass coverslips. Cell cultures were ester-loaded for 45 min with 10 µM Fluo-3-AM (Life Technologies) in HBSS with Ca^{2+} and Mg^{2+} (Life Technologies) supplemented with 25 mM HEPES (HBSS-HEPES) and 0.01% pluronic F-127 (Life Technologies) at room temperature, followed by de-esterification for 15 min. Subsequently, a fine narrow zone of cells was loaded with Bcl-2 peptides and the fluorescent dye Dextran TEXAS Red (100 µM; Life Technologies) using an *in situ* electroporation technique, as described previously (De Vuyst et al., 2008; Decrock et al., 2009; Monaco et al., 2012b; Decrock et al., 2014). Briefly, cells were rinsed three times with HBSS-HEPES followed by three washes with a low-conductivity electroporation buffer (4.02 mM KH_2PO_4, 10.8 mM K_2HPO_4, 1.0 mM $MgCl_2$, 300 mM sorbitol, 2.0 mM HEPES, pH 7.4). The cells were positioned 400 µm underneath a two-wire Pt-Ir electrode on the microscopic stage and electroporated in the presence of a tiny amount of electroporation solution (10 µl). Electroporation was performed with 50 kHz bipolar pulses at a field strength of 2000 V/cm and applied as 15 trains of 10 pulses of 2 ms duration each. After electroporation, cells were thoroughly washed with HBSS-HEPES and left 5 min to recover before proceeding with the Ca^{2+} imaging. For the latter, cells were superfused for 1 min with HBSS-HEPES, followed by 8 min with 1 mM caffeine in HBSS-HEPES. Imaging was carried out using an inverted Nikon Eclipse TE300 fluorescence microscope (Nikon, Brussels, Belgium) equipped with a ×40 oil immersion objective and an EM-CCD camera (QuantEM 512SC, Photometrics, Tuscon, AZ, USA). Images (one per second) were generated with custom-developed FluoFrames software written in Microsoft Visual C^{++} 6.0. Fluorescence-intensity changes in all cells were analyzed with FluoFrames software. For each individual trace, the relative change of Fluo-3 fluorescence $[(F-F_0)/F_0]$ was calculated. Subsequently, relative cytoplasmic $[Ca^{2+}]$ changes were quantified as the area under the curve of the separate Ca^{2+} traces. Data were normalized to the vehicle (DMSO) condition, which was set as 100%.

Fura-2-AM $[Ca^{2+}]$ measurements

A Zeiss Axio Observer Z1 Inverted Microscope equipped with a 20× air objective and a high-speed digital camera (Axiocam Hsm, Zeiss, Jena, Germany) were used. HEK RyR1 or HEK RyR3 cells co-transfected with 0.133 µg mCherry and 0.333 µg of the 3×FLAG constructs, and cells were loaded 2 days after transfection, at room temperature, using Fura-2-AM (1.25 µM; Biotium, Hayward, CA, USA) in modified Krebs buffer (135 mM NaCl, 6.2 mM KCl, 1.2 mM $MgCl_2$, 12 mM HEPES, pH 7.3, 11.5 mM glucose and 2 mM $CaCl_2$). After 30 min, de-esterification was allowed to occur for 30 min at room temperature. Before starting the $[Ca^{2+}]$ measurements, mCherry-positive cells were selected. During the experiment, 3 mM BAPTA (Alfa Aesar, Ward Hill, MA, USA) was added to buffer extracellular Ca^{2+}. Caffeine and thapsigargin (Alomone Labs, Jerusalem, Israel) responses were measured. For calibration, minimal and maximal Fura-2 responses were subsequently determined using 2 µM of ionomycin (Enzo Life Sciences, Farmingdale, NY, USA) supplemented with 50 mM EGTA or 500 mM $CaCl_2$, respectively, in modified Krebs buffer. When XeB (2 µM) was used, it was added to the cell medium 1 h prior to Fura-2-AM loading of the cell. XeB was also included during all steps of the loading process. The cytosolic $[Ca^{2+}]$ was calculated using $[Ca^{2+}]\ (nM)=K_d\times(F_{380max}/F_{380min})\times(R-R_{min})/(R_{max}-R)$, where K_d is the dissociation constant of Fura-2 for Ca^{2+} at room temperature (220 nM). In each experiment, 15–20 mCherry-positive cells were measured, which was repeated on at least three different days. Maximum peak values were calculated for each calibrated trace by subtracting the baseline $[Ca^{2+}]$ from the maximum response, followed by averaging individual data points. Replicate experiments

within the same day were also averaged and used for obtaining final averages for all days. For thapsigargin experiments, the area under the curve was determined by integrating the curves from the time point when thapsigargin was added, until calibration was started 10 min later.

Hippocampal [Ca^{2+}] measurements

At 1 week before measuring, a genetically encoded GCaMP3 Ca^{2+} indicator was introduced in the neurons by adenoviral infection. 14- to 18-day-old hippocampal neurons were used for these experiments. The coverslips were placed in the perfusion chamber of a Slice Scope microscope (Scientifica, East Sussex, UK). The neurons were perfused with heated (30°C), oxygenated artificial cerebrospinal fluid (aCSF) containing: 124 mM NaCl, 1.25 mM NaH_2PO_4, 3 mM KCl, 26 mM $NaHCO_3$, 2 mM $CaCl_2$, 1 mM $MgCl_2$ and 10 mM glucose at pH 7.4. Tetrodotoxin (1 µM) (Tocris Bioscience, Bristol, UK) was added just before use. Patch pipettes with a 4 MΩ resistance were pulled from borosilicate capillaries (Science Products GmBH, Hofheim, Germany). These were filled with the following solution: 115 mM $CsMeSO_3$, 20 mM CsCl, 10 mM HEPES, 2.5 mM $MgCl_2$, 4 mM Na_2-ATP, 0.4 mM Na_2-GTP, 10 mM Na-phosphocreatine and 0.1 mM EGTA. The vehicle (DMSO) or 20 µM of either the scrambled BH4-Bcl-2 or the BH4-Bcl-2 peptide was added to this solution just before the experiment. Utilizing whole-cell voltage clamp the membrane potential was clamped at −60 mV using a MultiClamp 700B amplifier (Molecular Devices, Biberach an der Riss, Germany). After 5 min of incubation with the peptide, the [Ca^{2+}] measurement was started. Using a pneumatic drug-ejection system (PDES-02DX from NPI, Tamm, Germany), a local 10 mM caffeine puff was administrated after 1 min through a second patch pipette positioned 15–25 µm from the cell. Imaging was performed using a CoolLED pE-2 excitation system (Life Sciences & Analytical, Andover, UK) in combination with an ORCA-Flash2.8 C11440-10C camera (Hamamatsu, Almere, The Netherlands). HCImage software (Hamamatsu) was used for analyzing the [Ca^{2+}] measurements.

Statistical analysis

When comparing two conditions, two-tailed unpaired Student's *t*-tests were performed. For comparing three or more groups, repeated measure ANOVA with Bonferroni post test was performed. Significance was taken at $P<0.05$. The exact *P*-values have been indicated in the figures, where feasible.

Acknowledgements

We would like to thank Karol Ondrias and Zuzana Tomaskova (Slovak Academy of Science, Slovak Republic) for the helpful discussions, and Marco Benevento, Martijn Selten, Wei Ba (Radboud University, The Netherlands), Lubica Malekova (Slovak Academy, Slovak Repbulic), Kirsten Welkenhuyzen, Giovanni Monaco, Marina Crabbé and Anja Florizoone (KU Leuven, Belgium) for their excellent technical assistance.

Competing interests

The authors declare no competing interests.

Author contributions

The study was conceived and originally designed by T.V., H.D.S., J.B.P. and G.B., with subsequent input by N.N.K for the use of hippocampal neurons. T.V. and E.D. performed the experiments. J.M. and V.S. contributed essential reagents and materials. T.V., E.D., L.M., L.L., H.D.S., N.N.K., J.B.P. and G.B. analyzed, interpreted and/or discussed the data. T.V. and G.B. drafted the manuscript. All authors critically revised the manuscript and approved the final article.

Funding

This work was supported by the Research Foundation-Flanders (FWO) [grant numbers G.0571.12 to G.B., H.D.S., J.B.P. and L.L., and G.0134.09N to L.L.]; by the Research Council of the KU Leuven (OT START) [grant number STRT1/10/044 to G.B.]; by the Interuniversity Attraction Poles Program (Belgian Science Policy) [grant numbers P7/13 to J.B.P., G.B. and L.M., and P7/10 to L.L.]; and by the Donders Center for Neuroscience fellowship award of the Radboud University Nijmegen Medical Center; and the FP7-Marie Curie International Reintegration Grant [grant number 277091] to N.N.K. T.V. was supported for his stay at the Radboud University by FWO travel grant [grant number V42613N].

Supplementary material

Supplementary material available online at
http://jcs.biologists.org/lookup/suppl/doi:10.1242/jcs.150011/-/DC1

References

Ahn, T., Yun, C. H., Kim, H. R. and Chae, H. J. (2010). Cardiolipin, phosphatidylserine, and BH4 domain of Bcl-2 family regulate Ca^{2+}/H^{+} antiporter activity of human Bax inhibitor-1. *Cell Calcium* **47**, 387-396.

Arbel, N. and Shoshan-Barmatz, V. (2010). Voltage-dependent anion channel 1-based peptides interact with Bcl-2 to prevent antiapoptotic activity. *J. Biol. Chem.* **285**, 6053-6062.

Arbel, N., Ben-Hail, D. and Shoshan-Barmatz, V. (2012). Mediation of the antiapoptotic activity of Bcl-xL protein upon interaction with VDAC1 protein. *J. Biol. Chem.* **287**, 23152-23161.

Balshaw, D. M., Xu, L., Yamaguchi, N., Pasek, D. A. and Meissner, G. (2001). Calmodulin binding and inhibition of cardiac muscle calcium release channel (ryanodine receptor). *J. Biol. Chem.* **276**, 20144-20153.

Berridge, M. J. (2011). Calcium signalling and Alzheimer's disease. *Neurochem. Res.* **36**, 1149-1156.

Berridge, M. J. (2013). Calcium regulation of neural rhythms, memory and Alzheimer's disease. *J. Physiol*. (Epub ahead of print).

Bezprozvanny, I., Watras, J. and Ehrlich, B. E. (1991). Bell-shaped calcium-response curves of Ins(1,4,5)P_3- and calcium-gated channels from endoplasmic reticulum of cerebellum. *Nature* **351**, 751-754.

Blayney, L., Beck, K., MacDonald, E., D'Cruz, L., Nomikos, M., Griffiths, J., Thanassoulas, A., Nounesis, G. and Lai, F. A. (2013). ATP interacts with the CPVT mutation-associated central domain of the cardiac ryanodine receptor. *Biochim. Biophys. Acta, Gen. Subj.* **1830**, 4426-4432.

Bonneau, B., Prudent, J., Popgeorgiev, N. and Gillet, G. (2013). Non-apoptotic roles of Bcl-2 family: the calcium connection. *Biochim Biophys Acta* **1833**, 1755-1765.

Brillantes, A. B., Ondrias, K., Scott, A., Kobrinsky, E., Ondriasová, E., Moschella, M. C., Jayaraman, T., Landers, M., Ehrlich, B. E. and Marks, A. R. (1994). Stabilization of calcium release channel (ryanodine receptor) function by FK506-binding protein. *Cell* **77**, 513-523.

Bround, M. J., Wambolt, R., Luciani, D. S., Kulpa, J. E., Rodrigues, B., Brownsey, R. W., Allard, M. F. and Johnson, J. D. (2013). Cardiomyocyte ATP production, metabolic flexibility, and survival require calcium flux through cardiac ryanodine receptors in vivo. *J. Biol. Chem.* **288**, 18975-18986.

Brunelle, J. K. and Letai, A. (2009). Control of mitochondrial apoptosis by the Bcl-2 family. *J. Cell Sci.* **122**, 437-441.

Bull, R., Finkelstein, J. P., Humeres, A., Behrens, M. I. and Hidalgo, C. (2007). Effects of ATP, Mg^{2+}, and redox agents on the Ca^{2+} dependence of RyR channels from rat brain cortex. *Am. J. Physiol.* **293**, C162-C171.

Bultynck, G., Rossi, D., Callewaert, G., Missiaen, L., Sorrentino, V., Parys, J. B. and De Smedt, H. (2001a). The conserved sites for the FK506-binding proteins in ryanodine receptors and inositol 1,4,5-trisphosphate receptors are structurally and functionally different. *J. Biol. Chem.* **276**, 47715-47724.

Bultynck, G., De Smet, P., Rossi, D., Callewaert, G., Missiaen, L., Sorrentino, V., De Smedt, H. and Parys, J. B. (2001b). Characterization and mapping of the 12 kDa FK506-binding protein (FKBP12)-binding site on different isoforms of the ryanodine receptor and of the inositol 1,4,5-trisphosphate receptor. *Biochem. J.* **354**, 413-422.

Chipuk, J. E. and Green, D. R. (2008). How do BCL-2 proteins induce mitochondrial outer membrane permeabilization? *Trends Cell Biol.* **18**, 157-164.

Chipuk, J. E., Moldoveanu, T., Llambi, F., Parsons, M. J. and Green, D. R. (2010). The BCL-2 family reunion. *Mol. Cell* **37**, 299-310.

De Vuyst, E., De Bock, M., Decrock, E., Van Moorhem, M., Naus, C., Mabilde, C. and Leybaert, L. (2008). In situ bipolar electroporation for localized cell loading with reporter dyes and investigating gap junctional coupling. *Biophys. J.* **94**, 469-479.

Decrock, E., De Vuyst, E., Vinken, M., Van Moorhem, M., Vranckx, K., Wang, N., Van Laeken, L., De Bock, M., D'Herde, K., Lai, C. P. et al. (2009). Connexin 43 hemichannels contribute to the propagation of apoptotic cell death in a rat C6 glioma cell model. *Cell Death Differ.* **16**, 151-163.

Decrock, E., De Bock, M., Wang, N., Bol, M., Gadicherla, A., Leybaert, L. (2014). Electroporation loading and flash photolysis to investigate intra- and intercellular Ca^{2+} signaling. In *Calcium Techniques: A Laboratory Manual* (ed. J. B. Parys, M. Bootman, D. I. Yule and G. Bultynck), pp. 93-112. Cold Spring Harbor, NY: Cold Spring Harb. Protoc.

Dias, J. M., Szegedi, C., Jóna, I. and Vogel, P. D. (2006). Insights into the regulation of the ryanodine receptor: differential effects of Mg^{2+} and Ca^{2+} on ATP binding. *Biochemistry* **45**, 9408-9415.

Ferdek, P. E., Gerasimenko, J. V., Peng, S., Tepikin, A. V., Petersen, O. H. and Gerasimenko, O. V. (2012). A novel role for Bcl-2 in regulation of cellular calcium extrusion. *Curr. Biol.* **22**, 1241-1246.

Furuichi, T., Kohda, K., Miyawaki, A. and Mikoshiba, K. (1994). Intracellular channels. *Curr. Opin. Neurobiol.* **4**, 294-303.

Gaburjakova, M., Gaburjakova, J., Reiken, S., Huang, F., Marx, S. O., Rosemblit, N. and Marks, A. R. (2001). FKBP12 binding modulates ryanodine receptor channel gating. *J. Biol. Chem.* **276**, 16931-16935.

Giorgi, C., Romagnoli, A., Pinton, P. and Rizzuto, R. (2008). Ca^{2+} signaling, mitochondria and cell death. *Curr. Mol. Med.* **8**, 119-130.

Hajnóczky, G., Csordás, G. and Yi, M. (2002). Old players in a new role: mitochondria-associated membranes, VDAC, and ryanodine receptors as

contributors to calcium signal propagation from endoplasmic reticulum to the mitochondria. *Cell Calcium* **32**, 363-377.

Hanson, C. J., Bootman, M. D., Distelhorst, C. W., Wojcikiewicz, R. J. and Roderick, H. L. (2008). Bcl-2 suppresses Ca^{2+} release through inositol 1,4,5-trisphosphate receptors and inhibits Ca^{2+} uptake by mitochondria without affecting ER calcium store content. *Cell Calcium* **44**, 324-338.

Hwang, J. H., Zorzato, F., Clarke, N. F. and Treves, S. (2012). Mapping domains and mutations on the skeletal muscle ryanodine receptor channel. *Trends Mol. Med.* **18**, 644-657.

Ikemoto, N. and Yamamoto, T. (2002). Regulation of calcium release by interdomain interaction within ryanodine receptors. *Front. Biosci.* **7**, d671-d683.

Jaimovich, E., Mattei, C., Liberona, J. L., Cardenas, C., Estrada, M., Barbier, J., Debitus, C., Laurent, D. and Molgó, J. (2005). Xestospongin B, a competitive inhibitor of IP_3-mediated Ca^{2+} signalling in cultured rat myotubes, isolated myonuclei, and neuroblastoma (NG108-15) cells. *FEBS Lett.* **579**, 2051-2057.

Kasri, N. N., Parys, J. B., Callewaert, G., Missiaen, L. and De Smedt, H. (2004). Calmodulin and calcium-release channels. *Biol. Res.* **37**, 577-582.

Kim, B. C., Kim, H. T., Mamura, M., Ambudkar, I. S., Choi, K. S. and Kim, S. J. (2002). Tumor necrosis factor induces apoptosis in hepatoma cells by increasing Ca^{2+} release from the endoplasmic reticulum and suppressing Bcl-2 expression. *J. Biol. Chem.* **277**, 31381-31389.

Kiviluoto, S., Vervliet, T., Ivanova, H., Decuypere, J. P., De Smedt, H., Missiaen, L., Bultynck, G. and Parys, J. B. (2013). Regulation of inositol 1,4,5-trisphosphate receptors during endoplasmic reticulum stress. *Biochim Biophys Acta* **1833**, 1612-1624.

Kuo, T. H., Kim, H. R., Zhu, L., Yu, Y., Lin, H. M. and Tsang, W. (1998). Modulation of endoplasmic reticulum calcium pump by Bcl-2. *Oncogene* **17**, 1903-1910.

Lanner, J. T., Georgiou, D. K., Joshi, A. D. and Hamilton, S. L. (2010). Ryanodine receptors: structure, expression, molecular details, and function in calcium release. *Cold Spring Harb. Perspect. Biol.* **2**, a003996.

Letai, A. G. (2008). Diagnosing and exploiting cancer's addiction to blocks in apoptosis. *Nat. Rev. Cancer* **8**, 121-132.

Liu, Z., Wang, R., Zhang, J., Chen, S. R. and Wagenknecht, T. (2005). Localization of a disease-associated mutation site in the three-dimensional structure of the cardiac muscle ryanodine receptor. *J. Biol. Chem.* **280**, 37941-37947.

Luciani, D. S., Gwiazda, K. S., Yang, T. L., Kalynyak, T. B., Bychkivska, Y., Frey, M. H., Jeffrey, K. D., Sampaio, A. V., Underhill, T. M. and Johnson, J. D. (2009). Roles of IP_3R and RyR Ca^{2+} channels in endoplasmic reticulum stress and beta-cell death. *Diabetes* **58**, 422-432.

Maes, K., Missiaen, L., Parys, J. B., De Smet, P., Sienaert, I., Waelkens, E., Callewaert, G. and De Smedt, H. (2001). Mapping of the ATP-binding sites on inositol 1,4,5-trisphosphate receptor type 1 and type 3 homotetramers by controlled proteolysis and photoaffinity labeling. *J. Biol. Chem.* **276**, 3492-3497.

Mak, D. O. and Foskett, J. K. (1998). Effects of divalent cations on single-channel conduction properties of Xenopus IP_3 receptor. *Am. J. Physiol.* **275**, C179-C188.

Martin, C., Chapman, K. E., Seckl, J. R. and Ashley, R. H. (1998). Partial cloning and differential expression of ryanodine receptor/calcium-release channel genes in human tissues including the hippocampus and cerebellum. *Neuroscience* **85**, 205-216.

Marx, S. O., Reiken, S., Hisamatsu, Y., Jayaraman, T., Burkhoff, D., Rosemblit, N. and Marks, A. R. (2000). PKA phosphorylation dissociates FKBP12.6 from the calcium release channel (ryanodine receptor): defective regulation in failing hearts. *Cell* **101**, 365-376.

Masumiya, H., Wang, R., Zhang, J., Xiao, B. and Chen, S. R. (2003). Localization of the 12.6-kDa FK506-binding protein (FKBP12.6) binding site to the NH2-terminal domain of the cardiac Ca^{2+} release channel (ryanodine receptor). *J. Biol. Chem.* **278**, 3786-3792.

Min, C. K., Yeom, D. R., Lee, K. E., Kwon, H. K., Kang, M., Kim, Y. S., Park, Z. Y., Jeon, H. and Kim, H. (2012). Coupling of ryanodine receptor 2 and voltage-dependent anion channel 2 is essential for Ca^{2}+ transfer from the sarcoplasmic reticulum to the mitochondria in the heart. *Biochem. J.* **447**, 371-379.

Monaco, G., Beckers, M., Ivanova, H., Missiaen, L., Parys, J. B., De Smedt, H. and Bultynck, G. (2012a). Profiling of the Bcl-2/Bcl-$X_{(L)}$-binding sites on type 1 $IP_{(3)}$ receptor. *Biochem. Biophys. Res. Commun.* **428**, 31-35.

Monaco, G., Decrock, E., Akl, H., Ponsaerts, R., Vervliet, T., Luyten, T., De Maeyer, M., Missiaen, L., Distelhorst, C. W., De Smedt, H. et al. (2012b). Selective regulation of IP_3-receptor-mediated Ca^{2+} signaling and apoptosis by the BH4 domain of Bcl-2 versus Bcl-Xl. *Cell Death Differ.* **19**, 295-309.

Nadif Kasri, N., Nakano-Kobayashi, A. and Van Aelst, L. (2011). Rapid synthesis of the X-linked mental retardation protein OPHN1 mediates mGluR-dependent LTD through interaction with the endocytic machinery. *Neuron* **72**, 300-315.

Oakes, S. A., Scorrano, L., Opferman, J. T., Bassik, M. C., Nishino, M., Pozzan, T. and Korsmeyer, S. J. (2005). Proapoptotic BAX and BAK regulate the type 1 inositol trisphosphate receptor and calcium leak from the endoplasmic reticulum. *Proc. Natl. Acad. Sci. USA* **102**, 105-110.

Plötz, M., Gillissen, B., Hossini, A. M., Daniel, P. T. and Eberle, J. (2012). Disruption of the VDAC2-Bak interaction by Bcl-$x_{(S)}$ mediates efficient induction of apoptosis in melanoma cells. *Cell Death Differ.* **19**, 1928-1938.

Quirion, J. C., Sevenet, T., Husson, H. P., Weniger, B. and Debitus, C. (1992). Two new alkaloids from Xestospongia sp., a New Caledonian sponge. *J. Nat. Prod.* **55**, 1505-1508.

Radermacher, M., Rao, V., Grassucci, R., Frank, J., Timerman, A. P., Fleischer, S. and Wagenknecht, T. (1994). Cryo-electron microscopy and three-dimensional reconstruction of the calcium release channel/ryanodine receptor from skeletal muscle. *J. Cell Biol.* **127**, 411-423.

Rong, Y. P., Aromolaran, A. S., Bultynck, G., Zhong, F., Li, X., McColl, K., Matsuyama, S., Herlitze, S., Roderick, H. L., Bootman, M. D. et al. (2008). Targeting Bcl-2-IP_3 receptor interaction to reverse Bcl-2's inhibition of apoptotic calcium signals. *Mol. Cell* **31**, 255-265.

Rong, Y. P., Bultynck, G., Aromolaran, A. S., Zhong, F., Parys, J. B., De Smedt, H., Mignery, G. A., Roderick, H. L., Bootman, M. D. and Distelhorst, C. W. (2009). The BH4 domain of Bcl-2 inhibits ER calcium release and apoptosis by binding the regulatory and coupling domain of the IP_3 receptor. *Proc. Natl. Acad. Sci. USA* **106**, 14397-14402.

Rossi, D., Simeoni, I., Micheli, M., Bootman, M., Lipp, P., Allen, P. D. and Sorrentino, V. (2002). RyR1 and RyR3 isoforms provide distinct intracellular Ca^{2+} signals in HEK 293 cells. *J. Cell Sci.* **115**, 2497-2504.

Ruiz, A., Matute, C. and Alberdi, E. (2009). Endoplasmic reticulum Ca^{2+} release through ryanodine and IP_3 receptors contributes to neuronal excitotoxicity. *Cell Calcium* **46**, 273-281.

Seo, M. D., Velamakanni, S., Ishiyama, N., Stathopulos, P. B., Rossi, A. M., Khan, S. A., Dale, P., Li, C., Ames, J. B., Ikura, M. et al. (2012). Structural and functional conservation of key domains in $InsP_3$ and ryanodine receptors. *Nature* **483**, 108-112.

Sharp, A. H., McPherson, P. S., Dawson, T. M., Aoki, C., Campbell, K. P. and Snyder, S. H. (1993). Differential immunohistochemical localization of inositol 1,4,5-trisphosphate- and ryanodine-sensitive Ca2+ release channels in rat brain. *J. Neurosci.* **13**, 3051-3063.

Van Acker, K., Bultynck, G., Rossi, D., Sorrentino, V., Boens, N., Missiaen, L., De Smedt, H., Parys, J. B. and Callewaert, G. (2004). The 12 kDa FK506-binding protein, FKBP12, modulates the Ca(2+)-flux properties of the type-3 ryanodine receptor. *J. Cell Sci.* **117**, 1129-1137.

Vanderheyden, V., Devogelaere, B., Missiaen, L., De Smedt, H., Bultynck, G. and Parys, J. B. (2009). Regulation of inositol 1,4,5-trisphosphate-induced Ca^{2+} release by reversible phosphorylation and dephosphorylation. *Biochim Biophys Acta* **1793**, 959-970.

White, C., Li, C., Yang, J., Petrenko, N. B., Madesh, M., Thompson, C. B. and Foskett, J. K. (2005). The endoplasmic reticulum gateway to apoptosis by Bcl-$X_{(L)}$ modulation of the $InsP_3R$. *Nat. Cell Biol.* **7**, 1021-1028.

Xiao, B., Masumiya, H., Jiang, D., Wang, R., Sei, Y., Zhang, L., Murayama, T., Ogawa, Y., Lai, F. A., Wagenknecht, T. et al. (2002). Isoform-dependent formation of heteromeric Ca2+ release channels (ryanodine receptors). *J. Biol. Chem.* **277**, 41778-41785.

Xu, Q. and Reed, J. C. (1998). Bax inhibitor-1, a mammalian apoptosis suppressor identified by functional screening in yeast. *Mol. Cell* **1**, 337-346.

Yamada, Y. and Mikoshiba, K. (2012). Quantitative comparison of novel GCaMP-type genetically encoded Ca^{2+} indicators in mammalian neurons. *Front Cell Neurosci.* **6**, 41.

Yamamoto, T. and Ikemoto, N. (2002). Spectroscopic monitoring of local conformational changes during the intramolecular domain-domain interaction of the ryanodine receptor. *Biochemistry* **41**, 1492-1501.

Yano, M. (2008). Ryanodine receptor as a new therapeutic target of heart failure and lethal arrhythmia. *Circ. J.* **72**, 509-514.

Zissimopoulos, S. and Lai, F. A. (2005a). Interaction of FKBP12.6 with the cardiac ryanodine receptor C-terminal domain. *J. Biol. Chem.* **280**, 5475-5485.

Zissimopoulos, S. and Lai, F. A. (2005b). Central domain of the human cardiac muscle ryanodine receptor does not mediate interaction with FKBP12.6. *Cell Biochem. Biophys.* **43**, 203-219.

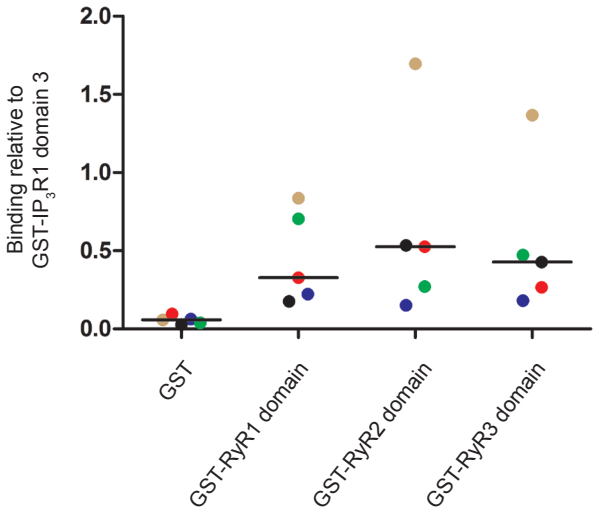

Supplementary figure 1: Quantification of the performed GST-pull downs. Each datapoint indicates the binding of 3XFLAG-Bcl-2 to the indicated GST domain normalized to the positive control, GST-IP_3R1 domain 3, which was set at 1. Pull downs performed during the same experiment are indicated by the same color. All individual data points are given together with the median (horizontal bar) (n=5).

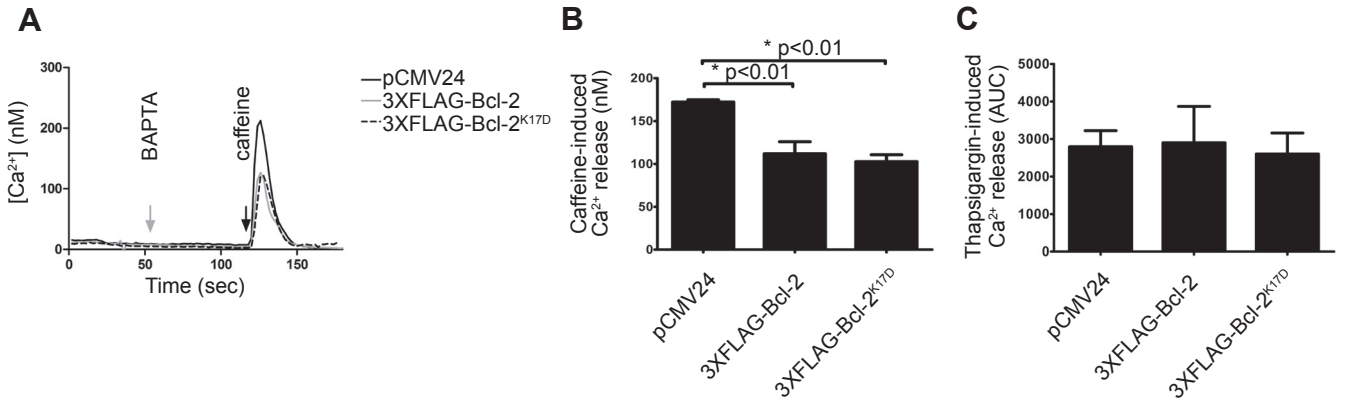

Supplementary figure 2: Fura-2 loaded, transfected (mCherry-positive) HEK RyR1 cells were selected for single-cell [Ca^{2+}] measurements. (A) Average [Ca^{2+}] traces (20 cells) from HEK RyR1 cells containing the pCMV24 vector, 3XFLAG-Bcl-2 or 3XFLAG-Bcl-2^{K17D} obtained in one experiment. The grey and black arrows respectively indicate the time points at which BAPTA (3 mM) or caffeine (4.5 mM) was administered. (B) Quantitative analysis of the caffeine responses in HEK RyR1 cells; values show averages ± s.e.m. of at least 3 independent experiments (n>80 cells). (C) Quantitative analysis of ER Ca^{2+}-store content. The ER Ca^{2+}-store content was determined similarly as in panel A, with the exception that thapsigargin (1 μM) was used instead of caffeine. The area under the curve (AUC) of the calibrated traces was used for determining the total ER Ca^{2+}-store content. The bar graph indicates the average AUC ± s.e.m. of at least 3 independent experiments (n>80 cells) for each condition.